Materials and Design Vol. 29 (8), pp. 1497 – 1503

The design of mosaic armour: the influence of tile-size on the ballistic performance

Paul J Hazell*, Colin J Roberson**, Mauricio Moutinho***

*Cranfield University, Defence Academy of the United Kingdom, Shrivenham, SN6 8LA, UK
**Advanced Defence Materials Ltd., Rugby, Warwickshire, CV21 3XH, UK
*** Brazilian Army, Rio de Janeiro, Brazil

ABSTRACT

Silicon carbide square tiles of different areal geometries and manufactured via two different processing routes have been bonded to polycarbonate layers to evaluate their ballistic performance. Four ceramic tile sizes were tested: 85mm, 60mm, 50mm and 33mm. In each case the residual depth-of-penetration into a polycarbonate semi-infinite backing was recorded. To elucidate the penetration and failure mechanisms, a computational model using the JH-1 ceramic model [23] of the projectile used in the experimental study penetrating into a silicon carbide-faced polycarbonate was implemented in the hydrocode AUTODYN-2D. This paper shows that there is a critical dimension of tile that should be used in a silicon carbide-based ceramic-faced mosaic armour system design to ensure optimum system performance when each tile is struck centrally.

Keywords: **A** engineering ceramics, **E** impact and ballistics, **H** failure analysis,

Materials and Design Vol. 29 (8), pp. 1497 – 1503

INTRODUCTION

The ballistic performance of ceramic materials using in armour applications is well known and has been extensively studied since the 1960s [1-10]. A ceramic-faced armour design usually consists of the hard disrupting face of the ceramic and some kind of absorbing element behind. The purpose of the ceramic is to induce fragmentation in the projectile or induce erosion thereby redirecting and dispersing the kinetic energy. The absorber on the other hand, acts to transfer the kinetic energy of the projectile to a lower form of energy – such as heat, through inelastic deformation (for example). Ceramics, are inherently brittle materials and consequently have fracture toughness (K_{Ic}) values in the 1-5 MPam^{½} range as opposed to the 5—170 MPam^{½} range for metals [11]. Consequently, when a projectile impacts and penetrates the ceramic face, brittle failure ensues leading to extensive fragmentation of the tile. If the fragments are not retained in place then the multi-hit capability of the armour is compromised.

Many modern-day armours are regularly subjected to automatic weapons fire where multiple bullets are fired towards a single location. Accordingly for multi-hit protection, it is necessary to retain as much ceramic material intact as possible after each subsequent hit. One of the ways that this can be achieved is by reducing the tile-size such that that if one tile has been destroyed protecting against a single projectile, the exposed area to subsequent strikes is minimized. Reducing the tile size inevitably leads to an increase in the number of interfaces between tiles for a given area. Bless and Jurick [12] have conducted a probability-based analysis of such mosaics to determine how multi-hit protection varies with tile size. They concluded that the impact of interfaces is likely for most armour system designs of interest. De Rosset [13] has also studied such patterned armours to examine the probability of defeating automatic weapons fire and similarly shown the vulnerability of joins between individual cells. However, for these

types of analyses there is a requirement to know how the ballistic performance is affected by the proximity of the impact to the tile edge. Without this knowledge, only crude assumptions can be made.

There is little published work in the open literature on the effect of tile size on the ballistic performance of ceramic-faced armours. Researchers have however, studied the effect of applying radial confinement to ceramic targets on their behaviour under dynamic loading conditions. The effect of the radial confinement on the behaviour of a ceramic tile has been studied by Sherman [14] who impacted a confined ceramic tile by a 0.30" armour piercing projectile. He showed that the addition of a steel confinement frame reduces the damage to the tile significantly whereas using other supporting materials of lower acoustic impedance leads to greater ceramic tile damage. Others have shown that the effect of adding steel radial confinement to ceramics subjected to high velocity long rod penetration also results in the resistance to penetration increasing [15,16].

The size of the tile is also important for ballistic testing of the ceramic. Good reviews of the various techniques are provided by James [17] and Normandia and Gooch [18]. There are clear advantages in using small tiles, not only in the cost of the ceramic but also the cost of the backing materials. Therefore it is advantageous to the design engineer to know the smallest tile-size that will provide the most accurate data on the material's ballistic resistance.

In most cost-effective mosaic armour designs, the sides of the tiles are unlikely to be ground flat and therefore there will be little or no intimate contact between each tile. Therefore to evaluate the worst case scenario it should be assumed that each tile is performing independently of its neighbour. In this work we have evaluated the effect of the proximity of a central impact point to a free surface on the ceramic armour's ballistic performance. Both the type of ceramic

and the size of the tile were varied. This work is part of a wider study on the resistance of ceramic-faced armour to penetration by tungsten-carbide cored projectiles.

EXPERIMENTAL SETUP

The depth-of-penetration technique as described by Rozenberg and Yeshurun [19] was used to measure the ballistic performance of the ceramic tiles (see Figure 1). In this work, polycarbonate was chosen as the backing material instead of more commonly used materials such as RHA or aluminium. The use of polycarbonate, which is less resistant to ballistic penetration, has the advantage that any small differences in the ballistic performance of the tile will result in relatively large differences in depth-of-penetration. Polycarbonate is clear so that analysis of depth-of-penetration can be done instantly without the requirement of X-Ray. It also has a similar acoustic impedance to the fibre composite used in light armour systems which leads to a more realistic trial than using a semi-infinite steel or aluminium backing. In these trials multiple polycarbonate tiles were used; each 100mm × 100mm ×12mm clamped together to form a semi-infinite target.

Materials and ammunition used

Two silicon carbides of varying sizes were tested: a direct sintered silicon carbide (Morgan AM&T PS-5000) and a commercially available liquid-phase-sintered (LPS) silicon carbide. These will be referred to as sSiC and LPS SiC in this paper. Their measured properties are presented in Table 1 along with the properties of polycarbonate taken from [20]. The elastic

properties of the silicon carbides were very similar. The densities were measured using a gas pycnometer and the longitudinal wave velocities, Young's modulus values and Poisson's ratios were measured ultrasonically using Panametrics' 5MHz longitudinal and shear-wave probes with the pulse-echo method. The true hardness values (HV_0) were calculated from a series of micro-hardness tests at different loads using an Indentec HWDM7. All ceramics tested were 7.5mm thick. The tiles were cut to 33×33mm, 51×51mm, 66×66mm and 85×85mm. A minimum of four tiles for each ceramic type and size were tested. Each ceramic tile was glued using Araldite AV4076-1 and HY4076 hardener mixed in the proportion of ten to four in weight. The surface of the polycarbonate was abraded in order to improve the gluing quality. A film of adhesive was applied on the ceramic surface which was then manually pressed against the polycarbonate and twisted until a continuous adhesive layer free of air bubbles was obtained. All the targets were glued and let to set at room temperature for at least 72 hours in an environment protected from light and moisture.

Figure 1 NEAR HERE.

Table 1 NEAR HERE.

Figure 2 shows the 7.62mm AP "Sniper 9" round core that was used for the ballistic tests. This projectile consists of a WC-Co cermet core placed in an aluminium cup and encased in a Cu-Zn jacket. The projectile's mass = 9.176g ±0.001g and measures 22.7mm in length and 7.8mm in diameter. The WC-Co core's mass = 5.556g ±0.001g and measures 22.3mm in length and 5.2mm in diameter with a 55° nose angle. The measured core hardness was 1292 ± 24

[HV2]. Chemical analysis of the core material revealed that it was of composition (weight percent) Co 11.6, C 5.4, Cu 0.1, balance W with no other element greater than 0.05 weight percent. The average muzzle velocity of this bullet was 838.0 m/s with a standard deviation of 5.3 m/s. The ammunition from our experimental set-up had an average dispersion of 4.3mm from the aim-point with a standard deviation of 2.5mm.

Figure 2 NEAR HERE.

After the tests, the polycarbonate was cut and the residual depth-of-penetration of the projectile in the backing material was measured and recorded. The distance from the impact point to the borders of the ceramic tile were also measured and recorded.

NUMERICAL MODEL

To elucidate the mechanisms of penetration and the effect of the tile edges on the penetrating projectile for the sSiC case we have conducted a series of computations. All computations were carried out using 2D axial symmetry using a Lagrangian mesh in the explicit non-linear transient dynamic numerical code - AUTODYN-2D. This software is explained in detail elsewhere [21] and a useful overview of these types of codes is provided by Anderson [22]. However in brief, this code solves the conservations laws of mass and momentum based on initial boundary conditions. The user is prompted for an equation of state that describes the pressure in terms of the internal energy and volume and a constitutive relationship that calculates the flow stress in

terms of a number of material and application-dependent parameters including strain, strain-rate and temperature. Failure models can be introduced to describe the failure.

Material models

To model the failure of the ceramic we used the Johnson-Holmquist strength and failure model – JH-1 [23]. The application of this material model in AUTODYN™ has been previously validated [24]. Data for this model has been acquired and successfully applied to simulate the dynamic response of glass [25], alumina [26,27], silicon carbide [23], and boron carbide [28,29]. A brief description of the model is given as follows: The schematic illustration of the JH-1 model from [23] is shown in Figure 2. The intact material strength is described as the linear segmented curve where the equivalent stress is a function of pressure. Any increase of strain rate under a given pressure increases the equivalent stress and therefore makes the material stronger. This is done according to

$$\sigma = \sigma_0 (1.0 + C \ln \dot{\varepsilon}) \qquad (1)$$

where $\dot{\varepsilon}$ is the strain rate, σ is the equivalent flow strength, σ_0 is the available strength at $\dot{\varepsilon} = 1.0$ and C is the strain rate constant. When damage to the ceramic occurs, the equivalent stress for a given pressure reduces and consequently the material becomes weaker. Damage (D) is defined as the ratio of the total accumulated increment of plastic strain and the equivalent failure strain. The material fails when either pressure reaches the tensile limit T or damage D is

equal to 1.0. After material is failed, it cannot withstand any tensile loading but can still withstand a limited compressive loading.

Figure 3 NEAR HERE

Modelling brittle materials is particularly troublesome as there is no experimental data available for the strength of the failed silicon carbide. Previous work [23] has centred around the penetration of SiC B – a pressure-assisted-densified silicon carbide manufactured by Cercom Inc. for which there is a reasonable amount of data on its dynamic behaviour. However, there is a paucity of similar data available for sintered silicon carbides. Consequently, no attempt has been made to derive a material model for our specific sintered silicon carbides.

Initial simulations with a ∅85 mm tile revealed that the current formulation of the JH-1 based on the SiC-B ceramic yielded a residual depth-of-penetration into the polycarbonate of 28 mm. This penetration depth was an over-prediction of the average experimental result of 15mm for the sSiC case. Consequently, we changed two parameters that have been used in [23] to define the strength of the damaged material (α and S^f_{max}). These parameters were not directly measured from laboratory tests but rather derived through computation of the sSiC experimental results. We have increased these values by simulating our experimental results from the penetration of the 7.5 mm thick 85 mm × 85 mm sSiC tile. This yielded values of $\alpha = 0.80$ and $S^f_{max} = 3.2$ GPa respectively to achieve a depth-of-penetration of 21 mm. The latter value (S^f_{max}) is particularly high however, given that we are simulating the failure of a different silicon carbide to the one reported in [23] and that the equivalent strength of damaged material can be higher than this value for other brittle materials [30,31] we feel justified in using this value in our

simulations.

There exists very little data on the dynamic behaviour of tungsten carbide too and, in particular the dynamic fracture characteristics that would lead to an appropriate material model.

Various attempts have been made in the past to model the failure of tungsten carbide materials that are subjected to shock loading. Both Aries *et al* [32] and Lopez Puente *et al* [33] have adopted the approach of Cortes *et al* [34]. In these works a model originally intended to model the failure of ceramics has been used. This involves the use of a pressure dependent yield surface and the evolution of damage that is associated with ceramic fragmentation through a calculated scalar damage parameter. In both cases they were modelling the penetration into a ceramic-faced composite armour using the LAPUA 7.62 mm armour piercing bullet.

Holmquist *et al* [35] adopted the approach of using both Johnson Cook fracture model [36] and a simple principal stress failure model for modelling the penetration of a tungsten carbide –cored projectile through a range of target materials. They concluded that the Johnson Cook fracture model represented the failure of the core. Their results showed good correlation of a 14.5 mm BS41 surrogate projectile penetrating monolithic and layered targets – including a ceramic- faced armour. Their material model for the tungsten carbide was based on a material with a 5.7% Co content that possessed a uniaxial compressive strength of 5.9 GPa [37]. However, tungsten carbide can demonstrate a range of strength properties depending on the Co content and the grain size [38]. Generally speaking, increasing the Co content affects the compressive strength. Consequently, we have not adopted Holmquist *et al*'s model for our core material as we have sought to choose from the literature data for a tungsten carbide that has a similar Co content. Early work by Johnson [39] presents data on a range of tungsten carbide materials with varying Co binder content and it was from this work that we drew our the material

model for the core. Under uniaxial compression, a tungsten carbide with a 10% wt Co content behaved according to:

$$\sigma = A + B\varepsilon_p^{\ n} \qquad (2)$$

where A is the yield strength at zero plastic strain, B is the strain hardening parameter and n is the strain hardening exponent. From [39], the values were A = 1.55 GPa, B = 22 and n = 0.45. In this work we have assumed that the strain-rate hardening effects of the tungsten carbide are small in comparison to the strain hardening effects and consequently they have been ignored. The tensile failure stress of the core material was also taken from [39] and was set to 1 GPa.

The gilding metal jacket was modelled assuming a flow stress of 575 MPa; this is consistent with the hardness measurements of the jacket before firing. Due to the face-centred cubic structure of this material and because it was heavily cold-worked during the bullet's manufacture, strain-rate effects were assumed to be zero. Further, we assumed an elastic-perfectly plastic behaviour. The strain-to-failure values for this type of cold-worked alloy are typically less than 5 % [40] and therefore a principle strain failure criteria was used that was set to this value.

The polycarbonate data was extracted from the AUTODYN™ material library [41]. This data was derived from [42]. The behaviour of the polycarbonate was modelled using a piecewise Johnson-Cook model and assumed to follow the stress-strain behaviour as defined by Table 2. The strain-rate strengthening behaviour was calculated according to Equation 1 with C = 0.040. Failure occurred when the effective plastic strain reached 200%.

The equation of state for the gilding metal and polycarbonate was of Mie-Grüneisen form [43] derived from a linear shock-particle Hugoniot thus:

$$U_s = c_0 + SU_p \tag{3}$$

where U_s and U_p are the shock and particle velocities respectively, c_0 is the bulk sound speed and S is the slope in the U_s versus U_p diagram. For the tungsten carbide core, no equation of state data was available for our particular alloy and therefore we adopted the equation of state from Holmquist *et al* [35].

For the silicon carbide, a polynomial equation of state was used when D<1.0 to define the pressure according to [23]

$$P = K_1\mu + K_2\mu^2 + K_3\mu^3 \tag{4}$$

where K_1 is the bulk modulus and K_2 and K_3 are material constants and μ is the material compression given by ρ/ρ_0 -1. When D=1.0, a bulking factor is added to Equation 4 to take into account the increase in local pressure due to material failure [23].

Material data for the gilding metal and polycarbonate was available in the AUTODYN material libraries and is presented in Table 3. Material model data for the silicon carbide is provided in Table 4.

Table 2 NEAR HERE.

Table 3 NEAR HERE.

Table 4 NEAR HERE.

Finally, cells were eroded according to a predetermined geometric strain value for each of the materials. These values were 250% for the silicon carbide and nominally 200% for the gilding metal, tungsten carbide and polycarbonate. A parametric investigation revealed that increasing the values in the core and the polycarbonate had little effect on the recorded depth-of-penetration into the polycarbonate or the penetration mechanism.

RESULTS AND DISCUSSION

Experimental

Below in Figure 5 are the recorded depth-of-penetration data for each of the ceramic-faced armour targets tested. Each reported data point refers to the average of the number of shots per tile and the error bars represent the spread in the data. Note that for the LPS SiC the depth-of-penetration is significantly higher than the sSiC and consequently represents a lower ballistic performance. It has been previously noted by Ray *et al* [44] that the ballistic efficiency of liquid-phase-sintered SiC against WC-Co projectiles is significantly less than for SiC made through alternative routes such as hot processing. Consequently, a thicker sample is required to shatter the projectile core. It has also been pointed out by Ray *et* al [44] that the measured depth of penetration using the DOP technique strongly correlates with the hardness of the ceramic. Given

that the LPS SiC has a lower hardness than the sSiC, our results are consistent with their results. It is also worth noting the spread of the data denoted by the error bars. For the sSiC targets the smaller targets exhibit more scatter in the results. However for the LPS SiC targets the scatter was fairly consistent from shot-to-shot. This pattern is also consistent with the core fragments that were recovered after each firing. Where the scatter was relatively large the fragments of the core could be recovered; where the scatter was small, the core had been mostly particulated (see Figure 4).

Figure 4 NEAR HERE.

Figure 5 NEAR HERE.

There appears to be little effect on the impact's proximity to the border for the LPS SiC material. Re-plotting Figure 5 in terms of the proximity of the impact to the sSiC ceramic tile's edge shows the border-effect more prominently. Here the data is presented as individual penetration depths.

Figure 6 NEAR HERE.

From the depth-of-penetration results presented in Figure 6 it can be seen that the sSiC ballistic performance was dependent of the distance from the impact point to the tile border. The performance increases as the impact occurs further from the border. The depth-of-penetration

into the polycarbonate rear layers after impacting the ceramic tile at 12 mm from the border was 43 mm. This was almost three-times the depth-of-penetration when the penetration was 42 mm from the closest border. For the sSiC beyond a critical distance, somewhere between 30 and 35 mm, the depth-of-penetration reached a consistent value (allowing for experimental scatter). At this location, the material's intrinsic ballistic performance was measured due to the absence of border effects.

With the sSiC tiles, fragments of the projectile could be recovered when the projectile completely penetrated a small tile of ceramic, but it was completely comminuted when the projectile completely penetrated an 85 mm tile. This explains the drop-off in depth-of-penetration with this ceramic as seen in Figure 6. The same does not occur with the liquid-phase-sintered tiles because there was little difference in the projectile's morphology during penetration regardless of the proximity of impact to a border. In this case, the recovered projectile was fragmented (see Figure 7 below).

Figure 7 NEAR HERE

Computational Model

The numerical study also demonstrated that a smaller tile resulted in less resistance to penetration. Figure 8 below shows a series of computational results from the penetration into the ceramic-faced polycarbonate target. There are a few observations to note from this computational model. Firstly, by 10 μs after impact the both the core and the jacket have failed resulting in the jacket flowing radially along the surface of the ceramic. By this time, stress

waves have been reflected from the ceramic / polycarbonate interface contributing to the damage. A coniod of damaged material has been formed below the penetrating core. The 33mm target possessed a slightly different form than that of the 85 mm target showing a two-step area of damaged had occurred at c. 1.5 mm from the rear surface. This is indicative of a stress wave reflecting off the periphery of the tile contributing to further damage. However, by 20 μs the 33 mm target exhibits a large amount of damage and radial displacement of the damaged material whereas the 85 mm target is largely retained intact. Between 10μs and 20μs the ∅33 mm target accrued damage at a faster rate than the ∅85mm target. The extent of the damage in the 33 mm target leads to a reduction in the erosion observed in the projectile and consequently more intact projectile is able to penetrate. Ultimately, the depth-of-penetration into the polycarbonate backing was 38 mm after completely penetrating the 7.5 mm thick ∅33 mm tile. The depth-of-penetration after completely penetrating a 7.5 mm thick ∅85 mm tile was 21 mm. Given that the simulations were calibrated by changing the strength characteristics of the damaged silicon carbide for a ∅85 mm tile, the depth of penetration for the ∅33 mm case is in good agreement with the sSiC experimental results shown in Figure 6 above.

Figure 8 NEAR HERE.

The ∅85 mm target appears to show considerable dwell in the initial 10-20 μs. This is consistent with results from other researchers that have studied the penetration into similar thicknesses of silicon carbide by small arms projectiles [23]. Whereas the degree of dwell induced by the 33 mm tile is significantly less by virtue of the earlier onset of damage. Our simulations of the penetration into a 7.5 mm thick ∅33 mm tile showed that by 20 μs, the strength of the material

towards the periphery of the tile reduced to zero. This was due to the release of pressure due to the proximity of the free surface. Towards the centre of the tile, the pressure was c. 0.2-0.4 GPa due to the penetrating projectile. Whereas with the 7.5 mm ∅85 mm tile the strength measured at 16.5 mm from the axis of penetration was c. 2-3 GPa; pressure along the axis of penetration was considerably higher than with the 33 mm tile and was computed to be 4-8 GPa close to the contact interface between the projectile and the target. Consequently, retaining the comminuted ceramic in place by virtue of the inertial confinement offered by the larger tile resulted in an increased computed pressure and consequently an increased computed strength of the damaged material.

CONCLUSIONS

Experiments have been carried out on two differently made silicon carbides to evaluate the effect of border proximity on each material's ballistic performance. Further, a series of computations have been carried out using a commercial hydrocode to elucidate the penetration mechanism in two different areal sizes of tile.

- The measured depth-of-penetration after completely penetrating 7.5-mm thick sSiC was dependent on the tile size. For this ceramic, the effect of the border was insignificant at a proximity of impact of approximately 30-35mm. Consequently, the minimum square tile-size that should be used so that the intrinsic ballistic properties of this material can be tested is 70mm × 70mm. For a central impact on a ceramic tile used in a mosaic armour design, this was assumed to be the worst case scenario where each tile was assumed to be performing independently of its neighbour.

- The sSiC out-performed the LPS SiC ballistically in the depth-of-penetration-test configuration.
- The LPS SiC tile showed little variation of ballistic performance with tile size. We believe that this was because the 85 mm ceramic was not able to damage the projectile's core to any great extent.
- The computational model was able to predict the depth-of-penetration into the polycarbonate after completely penetrating a 7.5 mm thick, 33 mm × 33 mm tile. It showed that the ∅33 mm tile accrued damage at a higher rate than the ∅85 mm tile. Further, it showed that the strength of the failed damage material was considerably reduced by virtue of the relatively close proximity of the radial boundary.

ACKNOWLEDGEMENTS

Some of this work was carried out during Capt Moutinho's study for a Forensic Engineering and Science MSc at Cranfield University. We would like to thank the Brazilian Army for funding his studies. We would also like to acknowledge Mr David Miller, Mr Gary Cooper and Mr Adrian Mustey for their technical assistance. Finally, our thanks to Morgan AM&T for supplying the samples and funding other materials used in the project.

REFERENCES

[1] Wilkins ML, Honodel CA, Swale D, An Approach to the Study of Light Armour, Lawrence Radiation Laboratory, Livermore, UCRL-50284, June (1967).

[2] Wilkins ML, Cline CF, and Honodel CA, Fourth Progress Report of Light Armour Program, Lawrence Radiation Laboratory, Livermore, UCRL-50694 (1969).

[3] Wilkins ML, Landingham RL, Honodel CA, Fifth Progress Report of Light Armour Program, Lawrence Radiation Laboratory, Livermore, UCRL-50980, January (1971).

[4] Cline CF, Wilkins ML, "The importance of material properties in ceramic armour", Proceedings of the Ceramic Armour Technology Symposium (USA), pp. 13–18, January (1969).

[5] Sadanandan S, Hetherington JG, Characterisation of ceramic/steel and ceramic/aluminium armours subjected to oblique impact. Int J Impact Engng 1997; 19:811-9.

[6] Hetherington JG, The optimization of two component composite armours. Int J Impact Eng 1992;12:409-14.

[7] Hetherington JG, Rajagopalan BP, An investigation into the energy absorbed during ballistic perforation of composite armours. Int J Impact Engng 1991; 11:33-40.

[8] Horsfall I, Buckley D, The effect of through-thickness cracks on the ballistic performance of ceramic armour systems, Int J Impact Engng 1996;18:309-18.

[9] Edwards MR. Land-based military applications. In: Bader MG, Kedward KT and Sawada Y, editors. Comprehensive Composite Materials, Oxford:Elsevier Science; 2000 p. 681-99.

[10] Hazell PJ, Fellows NA, Hetherington JG, A note on the behind armour effects from perforated alumina/aluminium targets. Int J of Impact Engng 1998;21:589-95.

[11] Ashby MF, Jones DRH, Engineering materials 2: An introduction to microstructures, processing and design. Oxford: Pergamom;1988.

[12] Bless SJ, Jurick DL, Design for multi-hit protection. Int J Impact Eng 1998; 21:905-8.

[13] de Rosset WS, Patterned armor performance evaluation. Int J Impact Engng 2005; 31:1223-34.

[14] Sherman D. Impact failure mechanisms in alumina tiles on finite thickness support and the effect of confinement. Int J of Impact Engng 2000;24:313-28.

[15] Partom Y, Littlefield DL. Validation and calibration of a lateral confinement model for long-rod penetration at ordnance and high velocities. Int J of Impact Engng 1995; 17:615-26.

[16] Lynch NJ, Bless SJ, Cullis IG, Berry D. The influence of confinement on the penetration of ceramic targets by KE projectiles at 1.8 and 2.6 km/s, Int J of Impact Engng 2006;33:390-401.

[17] James B, Depth of penetration testing. In: McCauley JW, Crowson A, Gooch Jr. WA, Rajendran AM, Bless SJ, Logan KV, Normandia M, Wax S, editors, Ceramic Armor Materials by Design, Ceramic Transactions, Vol.134, 2002, p. 165-72.

[18] Normandia MJ, Gooch WA, An overview of ballistic testing methods of ceramic materials. In: McCauley JW, Crowson A, Gooch Jr. WA, Rajendran AM, Bless SJ, Logan KV, Normandia M, Wax S, editors, Ceramic Armor Materials by Design, Ceramic Transactions, Vol.134, 2002 p.113-38.

[19] Rozenberg Z, Yeshurun Y, The relationship between ballistic efficiency and compressive strength of ceramic tiles. Int J Impact Engng 1988, 7:357-62.

[20] Millett JCF, Bourne NK, Shock and release of polycarbonate under one-dimensional strain. J Mater Sci 2006; 41:1683-90.

[21] Robertson N, Hayhurst C, Fairlie G, Numerical simulation of impact and fast transient phenomena using AUTODYN(TM)-2D and 3D. Nuclear Engineering and Design 1994; 150:235-241.

[22] Anderson, Jr. CE, An overview of the theory of hydrocodes. Int J of Impact Engng 1987;5:33-59.

[23] Holmquist TJ, Johnson GR, Response of silicon carbide to high velocity impact", J of Appl Phys 2002;91:5858–66.

[24] Quan X, Clegg RA, Cowler MS, Birnbaum NK, Hayhurst CJ, Numerical simulation of long rods impacting silicon carbide targets using JH-1 model. Int J Impact Engng 2006; 33:634-44.

[25] Holmquist TJ, Johnson GR, Grady DE, Lopatin CM, Hertel Jr. ES, High strain rate properties and constitutive modeling of glass. Proceedings of the 15th International Symposium on Ballistics, Jerusalem, Israel, 21–24 May, (1995).

[26] Anderson Jr. CE, Johnson GR, Holmquist TJ, Ballistic experiments and computations of confined 99.5% Al2O3 ceramic tiles. Proceedings of the 15th International Symposium on Ballistics, Jerusalem, Israel, 21–24 May, (1995).

[27] Westerling L, Lundberg P, The influence of confinement on the protective capability of ceramic armour at two different velocities. Proceedings of the 15th International Symposium on Ballistics, Jerusalem, Israel, 21–24 May, (1995).

[28] Johnson GR, Holmquist TJ, Response of boron carbide subjected to large strains, high strain rates, and high pressures, J of Appl Phys 1999; 85:8060–73.

[29] Westerling L, Lundberg P, Lundberg B. Tungsten long rod penetration into confined cylinders of boron carbide at and above ordnance velocities. Int J of Impact Engng 2001;25:703–14.

[30] Johnson GR, Holmquist TJ. Some observations on the strength of failed ceramic. In : Swab JJ, Zhu D, Kriven WM, editors. Advances in Ceramic Armor, Ceramic Engineering and Science Proceedings 2006; 26, (7), p. 3-10.

[31] Walker JD. Analytically Modeling Hypervelocity Penetration of Thick Ceramic Targets, Int J of Impact Engng 2003;29:747-55.

[32] Arias A, Zaera R, Lopez-Puente J, Navarro C. Numerical modeling of the impact behavior of new particulate-loaded composite materials. Composite Structures 2003;61:151–159.

[33] López-Puente J, Arias A, Zaera R, Navarro C. The effect of the thickness of the adhesive layer on the ballistic limit of ceramic/metal armours. An experimental and numerical study. Int J of Impact Engng 2005;32:321-36.

[34] Cortés R, Navarro C, Martínez MA, Rodríguez J, Sánchez-Gálvez V. Numerical modelling of normal impact on ceramic composite armours. Int J Impact Eng 1992; 12:639–51.

[35] Holmquist TJ, Johnson GR, Gooch WA. Modeling the 14.5 mm BS41 projectile for ballistic impact conditions. WIT Transactions on Modelling and Simulation 2005;40:61-75.

[36] Johnson GR, Cook WH, Fracture characteristics of three metals subjected to various strains, strain rates, temperatures and pressures. Eng Fract Mech 1985;21:31-48.

[37] Grady D. Impact failure and fragmentation properties of tungsten carbide. Int J of Impact Engng 1999; 23:307-317.

[38] Okamoto S, Nakazono Y, Otsuka K, Shimoitani Y, Takada J. Mechanical properties of WC/Co cemented carbide with larger WC grain size. Materials Characterization 2005;55:281-287.

[39] Johnson Jr., A. E. Mechanical properties at room temperature of four cermets of tungsten carbide with cobalt binder, National Advisory Committee for Aeronautics, Technical Note: 3309, Washington, USA, (1954).

[40] Properties and Selection: Nonferrous Alloys and Special-purpose Materials, Metals Handbook, Vol 2, 10th Edition, ASM International (1990).

[41] AUTODYN™, Century Dynamics Limited, Suite 1, 3 Horsham Gates, North Street, Horsham, West Sussex, UK, RH13 5PJ.

[42] Walley SM, Field JE, Strain rate sensitivity of polymers in compression from low to high rates, DYMAT 1994;J 1:211–27.

[43] Meyer MA, Dynamic behaviour of materials. New York: John Wiley & Sons; 1994.

[44] Ray D, Flinders R, Anderson A, Cutler R. Effect of room-temperature hardness and toughness on the ballistic performance of SiC-based ceramics. Ceram Sci Eng Proc 2005; 26 [7]:131-42.

LIST OF FIGURE CAPTIONS

Figure 1: The depth-of-penetration technique; t_c = tile thickness, P_r = depth-of-penetration.

Figure 2: The 7.62mm AP Sniper 9 ammunition showing the WC-Co core and the aluminium cup.

Figure 3: The JH-1 constitutive model from [23].

Figure 4: Crater formed in the polycarbonate after completely penetrating an 85 mm sSiC tile. Here the core was mostly particulated during the penetration of the ceramic.

Figure 5: Depth-of-penetration results for the sSiC and LPS SiC ceramic-faced targets.

Figure 6: Depth–of-penetration results for the sSiC-faced target (left) and the LPS SiC (right).

Figure 7: Recovered fragments of core after completely penetrating an 85 mm LPS SiC tile (middle) and a 33 mm LPS SiC tile (right). An intact projectile core is added for comparison (left).

Figure 8: Computational results showing the initial stages of penetration into the ceramic-faced polycarbonate. The left hand side of the images shows the results from the 85 mm tile whereas the right hand side of the images shows the results from 33mm tile. The depth of the polycarbonate has been truncated for clarity.

Table 1: Measured properties of the silicon carbides used in this trial; the data for the polycarbonate is taken from [20].

Ceramic	ρ_0 (kg/m^3)	c_L (m/s)	E (GPa)	ν	HV_0
sSiC	3147	12021	427.0	0.16	2400
LPS SiC	3252	12111	446.0	0.17	2089
Polycarbonate	1190	2130	2.6	0.40	-

Table 2: Plastic flow data for polycarbonate taken from the AUTODYN™ material library.

Effective plastic strain	Corresponding equivalent stress (MPa)
0.0	80.6
0.1	88.0
0.5	142.5
0.6	168.0
0.7	187.0

Table 3: Hydrodynamic data for the tungsten carbide, gilding metal and the polycarbonate.

	Notation	Tungsten carbide	Gilding metal (Copper)	Polycarbonate
Reference density (kg/m^3)	ρ_0	14770	8930	1190
Bulk sound speed (m/s)	c_0	-	3940	1933
Slope in U_s versus U_p diagram	S	-	1.489	2.65
Grüneisen coefficient	Γ	1.0	2.02	0.61
Bulk modulus (GPa)	K_1	362	-	-
Pressure coefficient (GPa)	K_2	694	-	-
Pressure coefficient (GPa)	K_3	0	-	-

Table 4: Johnson-Holmquist parameters used to model the behaviour of the silicon carbide.

Property	Notation	Value
Reference density (kg/m^3)	P_0	3215
Bulk modulus (GPa)	K_1	220
Shear modulus (GPa)	G	193
Hugoniot elastic limit (GPa)	HEL	11.7
Tensile strength (GPa)	T	0.75
Intact strength coefficient (GPa)	S_1	7.1
Intact strength coefficient (GPa)	P_1	2.5
Intact strength coefficient (GPa)	S_2	12.2
Intact strength coefficient (GPa)	P_2	10.0
Strain rate coefficient	C	0.009
Failed strength coefficient (GPa)	S^f_{max}	3.2
Failed strength coefficient	α	0.80
Pressure coefficient (GPa)	K_2	361
Pressure coefficient (GPa)	K_3	0
Damage coefficient	ϕ	0.012
Damage coefficient	ε^f_{MAX}	1.2
Damage coefficient (GPa)	P_3	99.75

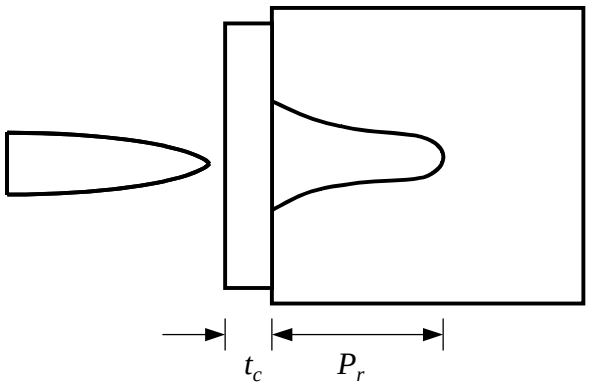

Figure 1: The depth-of-penetration technique; t_c = tile thickness, P_r = depth-of-penetration.

Figure 2: The 7.62mm AP Sniper 9 ammunition showing the WC-Co core and the aluminium cup.

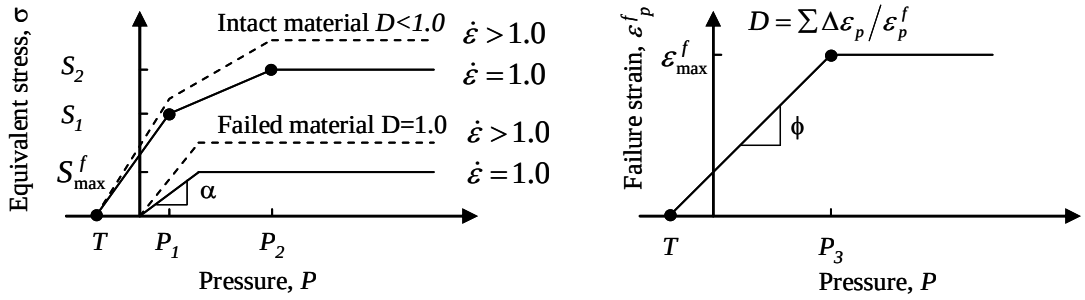

Figure 3: The JH-1 constitutive model from [23].

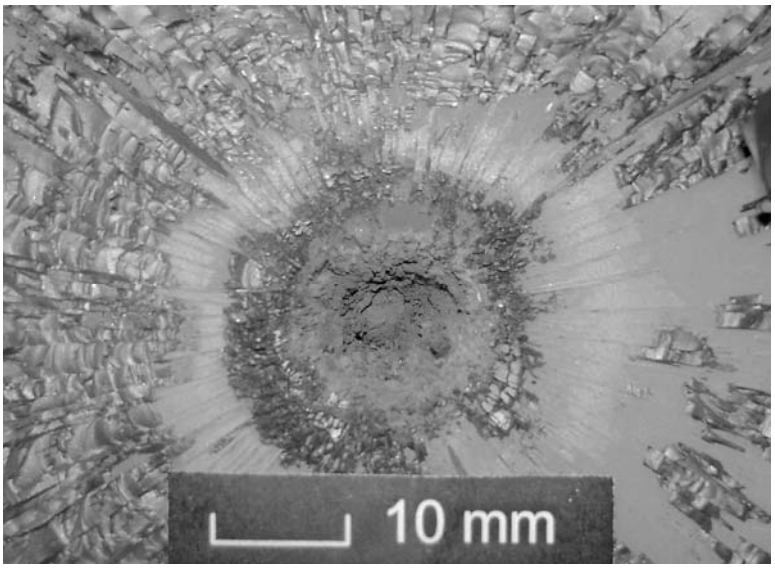

Figure 4: Crater formed in the polycarbonate after completely penetrating an 85 mm sSiC tile . Here the core was mostly particulated during the penetration of the ceramic.

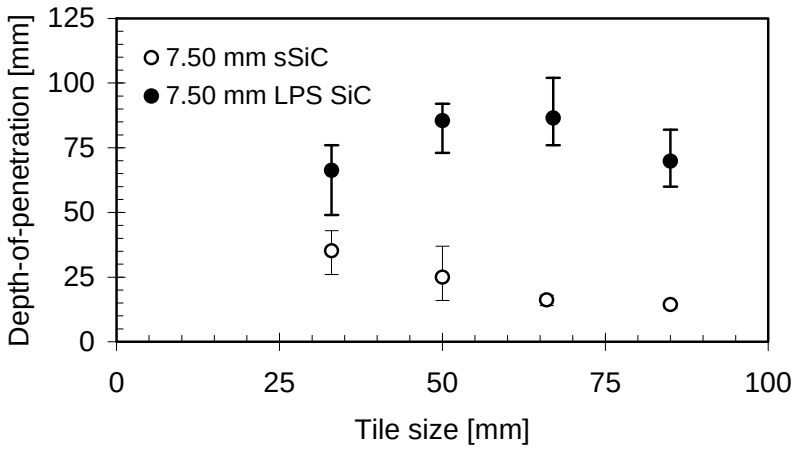

Figure 5: Depth-of-penetration results for the sSiC and LPS SiC ceramic-faced targets.

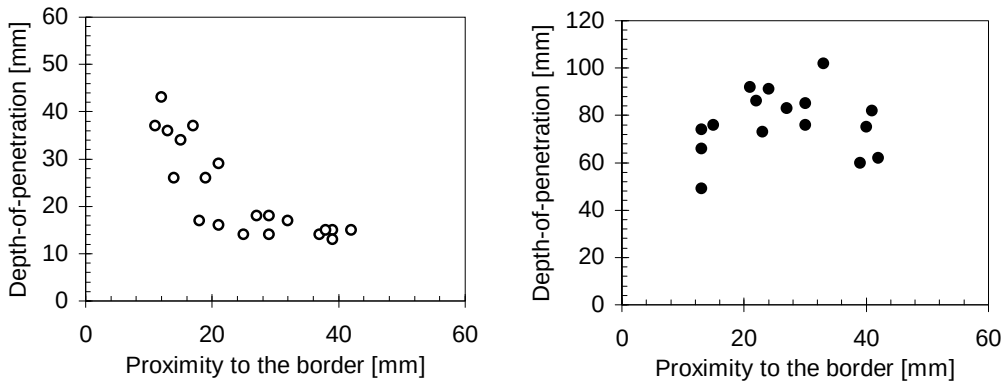

Figure 6: Depth–of-penetration results for the sSiC-faced target (left) and the LPS SiC (right).

Figure 7: Recovered fragments of core after completely penetrating an 85 mm LPS SiC tile (middle) and a 33 mm LPS SiC tile (right). An intact projectile core is added for comparison (left).

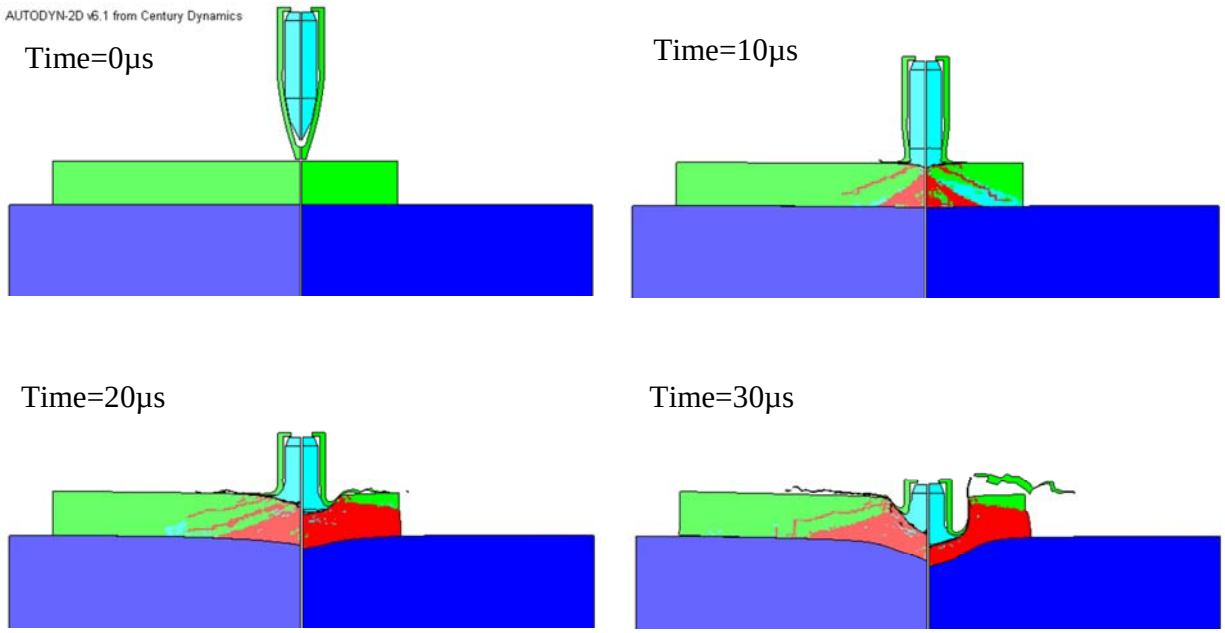

Figure 8: Computational results showing the initial stages of penetration into the ceramic-faced polycarbonate. The left hand side of the images shows the results from the 85 mm tile whereas the right hand side of the images shows the results from 33mm tile. The depth of the polycarbonate has been truncated for clarity.